Molecular Therapy
Nucleic Acids
Original Article

METTL3 Facilitates Oral Squamous Cell Carcinoma Tumorigenesis by Enhancing c-Myc Stability via YTHDF1-Mediated m^{6}A Modification

Wei Zhao,[1,4] Yameng Cui,[2,4] Lina Liu,[3,4] Xiaozhou Ma,[1] Xiaoqian Qi,[1] Yue Wang,[1] Zihao Liu,[1] Shiqing Ma,[1] Jingwen Liu,[1] and Jie Wu[1]

[1]The School and Hospital of Stomatology, Tianjin Medical University, Tianjin 300070, China; [2]Department of Integrative Oncology, Tianjin Medical University Cancer Institute and Hospital, Tianjin, China; [3]Department of Prosthodontics, Tianjin Stomatological Hospital, Hospital of Stomatology, NanKai University, Tianjin 300041, China

N^6-Methyladenosine (m^{6}A) is the most common internal modification of eukaryotic messenger RNA (mRNA) that occurred on the N^6 nitrogen of adenosine. However, the roles of m^{6}A in oral squamous cell carcinoma (OSCC) are still elusive. Here, we investigate the function and mechanism of methyltransferase-like 3 (METTL3) in OSCC tumorigenesis. Clinically, METTL3 was significantly upregulated in tissue samples and correlated with the poor prognosis of OSCC patients. Functionally, loss and gain studies illustrated that METTL3 promoted the proliferation, invasion, and migration of OSCC cells in *vitro*, and METTL3 knockdown inhibited tumor growth *in vivo*. Mechanistically, methylated RNA immunoprecipitation sequencing (MeRIP-seq) illustrated that METTL3 targeted the 3′ UTR (near to stop codon) of the c-Myc transcript to install the m^{6}A modification, thereby enhancing its stability. Furthermore, results revealed that YTH N^6-methyladenosine RNA binding protein 1 (YTH domain family, member 1 [YTHDF1]) mediated the m^{6}A-increased stability of c-Myc mRNA catalyzed by METTL3. In conclusion, our findings herein identify that METTL3 accelerates the c-Myc stability via YTHDF1-mediated m^{6}A modification, thereby giving rise to OSCC tumorigenesis.

INTRODUCTION

Oral squamous cell carcinoma (OSCC) is one of the most common cancers of the oral or head-and-neck region, accounting for approximately 90% of oral neoplasms and 3% of systemic malignancy.[1,2] OSCC is always characterized by the high metastatic, high recurrence, and poor prognosis in clinical treatment.[3] Although great progress has been made for the therapeutic strategy during the past decades, the prognosis of OSCC individuals is still poor.[4,5] It is reported that the pathogenesis of OSCC is involved with diverse risk factors and mechanisms that trigger the recurrence and metastasis of OSCC.

N^6-Methyladenosine (m^{6}A) is one of the most abundant internal modifications in eukaryotic messenger RNA (mRNA) that plays critical roles in gene-expression regulation, including stability, splicing, and translation.[6] In the overall statistic, there are around 25% of mRNAs containing at least one m^{6}A nucleotide site, especially at the adenosine.[7] m^{6}A is specifically catalyzed at the consensus motif DRACH (where D = A/G/U, R = A/G, and H = A/C/U). In addition to m^{6}A, there are other types of post-transcriptional modifications, including 5-methylcytosine (m^{5}C) and pseudouridine (ψ).[8,9] To detect the regions harboring m^{6}A (m^{6}A peaks), researchers developed immunoprecipitation-based approaches coupled with high-throughput sequencing (m^{6}A-seq, m^{6}A-methylated RNA immunoprecipitation [MeRIP]) with high accuracy.[10] Besides, it could also perform UV crosslinking to covalently bind the anti-m^{6}A antibody (referred to as methylation individual-nucleotide-resolution crosslinking and immunoprecipitation [miCLIP]) for identification of single-modified nucleotides within RNA species.[11]

m^{6}A modification is a dynamic and reversible process mediated by three m^{6}A key elements: "writers," "erasers," and "readers."[12] It is catalyzed mainly by the RNA methyltransferase complex (writers), including methyltransferase-like 3 and 4 (METTL3 and METTL14) and Wilms' tumor 1-associated protein (WTAP).[13] The methylation is removed by the RNA demethylases (erasers), including fat mass and obesity-associated protein (FTO) and alkB homolog 5 (ALKBH5).[14] In this process, the m^{6}A reader proteins are also essential, including YTH domain family (YTHDF), insulin-like growth factor 2 mRNA binding protein 2 (IGF2BP), and HNRNPA2B1. Current research indicates that METTL3 is responsible for catalyzing m^{6}A installation,[15] METTL14 is involved in interacting with target mRNA,[16] and WTAP is in charge of the localization in the nuclear speckle.[17] YTHDF proteins are identified as a reader of m^{6}A to regulate the stability of m^{6}A-bearing transcripts. These elements of m^{6}A have been found to significantly regulate the human tumorigenesis origination, such as acute myeloid leukemia,[7,18] gastric cancer,[19] breast cancer,[20] and pancreatic cancer,[21] et al.

Received 26 October 2019; accepted 28 January 2020;
https://doi.org/10.1016/j.omtn.2020.01.033.

[4]These authors contributed equally to this work.

Correspondence: Jingwen Liu, The School and Hospital of Stomatology, Tianjin Medical University, Qixiangtai Road, No. 12, Tianjin 300070, China.
E-mail: liujingwen@tmu.edu.cn
Correspondence: Jie Wu, The School and Hospital of Stomatology, Tianjin Medical University, Qixiangtai Road, No. 12, Tianjin 300070, China.
E-mail: wujiedoctor@tmu.edu.cn

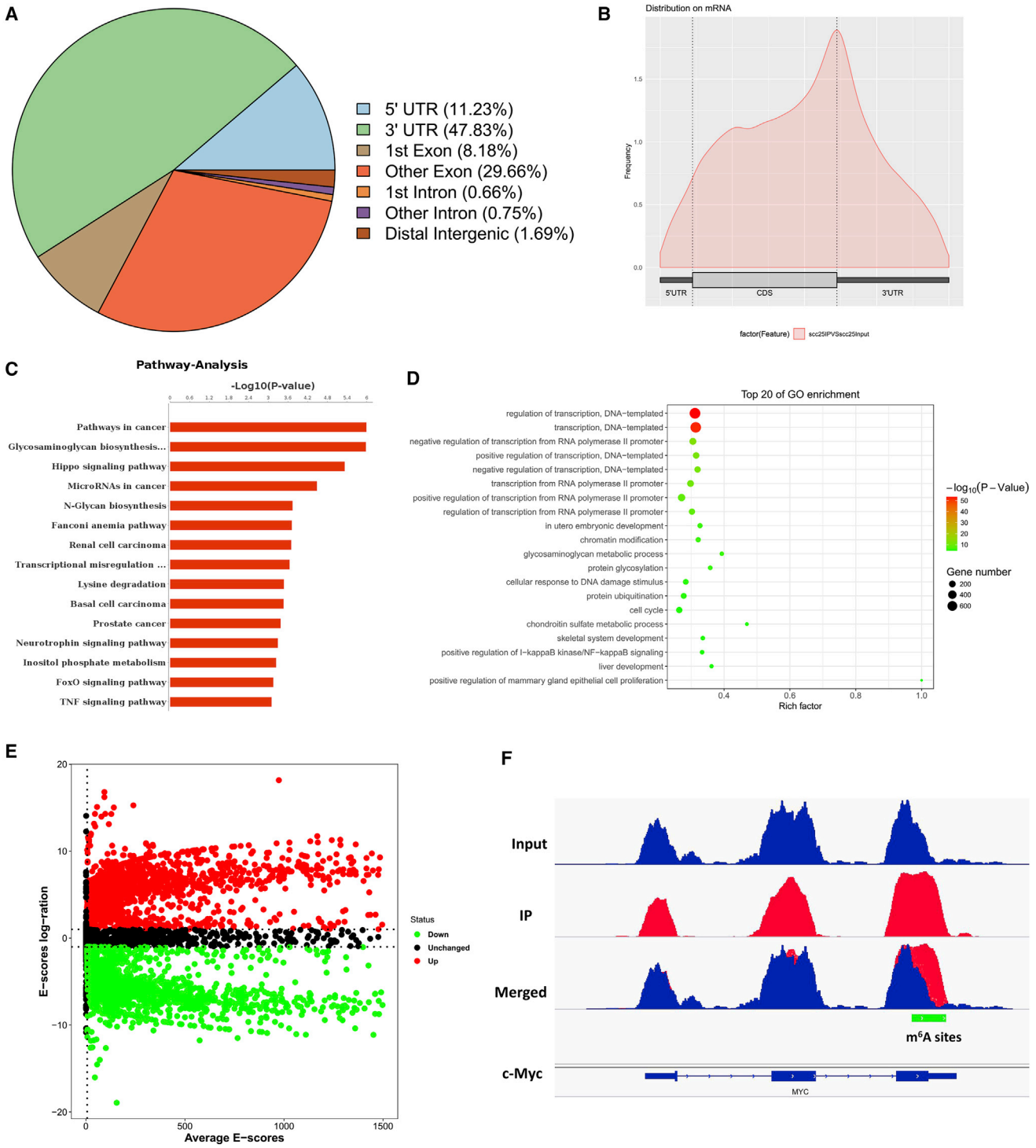

Figure 1. MeRIP-Seq Analysis Unveils the m^{6}A Profiles in the OSCC Cells

(A) m^{6}A-RNA immunoprecipitation sequencing (MeRIP-seq) was performed. Metagene profile illustrated the m^{6}A distribution in 5′ untranslated region (UTR), coding sequences (CDS), stop codon, and 3′ UTR. (B) Metagene profile of m^{6}A distribution showed the m^{6}A peaks in the stop codon, including the CDSs and 3′ UTRs. (C) Pathway analysis showed the potential pathway for the OSCC. (D) Gene Ontology (GO) analysis showed the target manners for the OSCC. (E) Volcano plot for MeRIP-seq analysis showed the different expression of transcripts, including upregulated and downregulated transcripts. (F) The Integrative Genomics Viewer (IGV) tool revealed the m^{6}A peak distribution c-Myc mRNA.

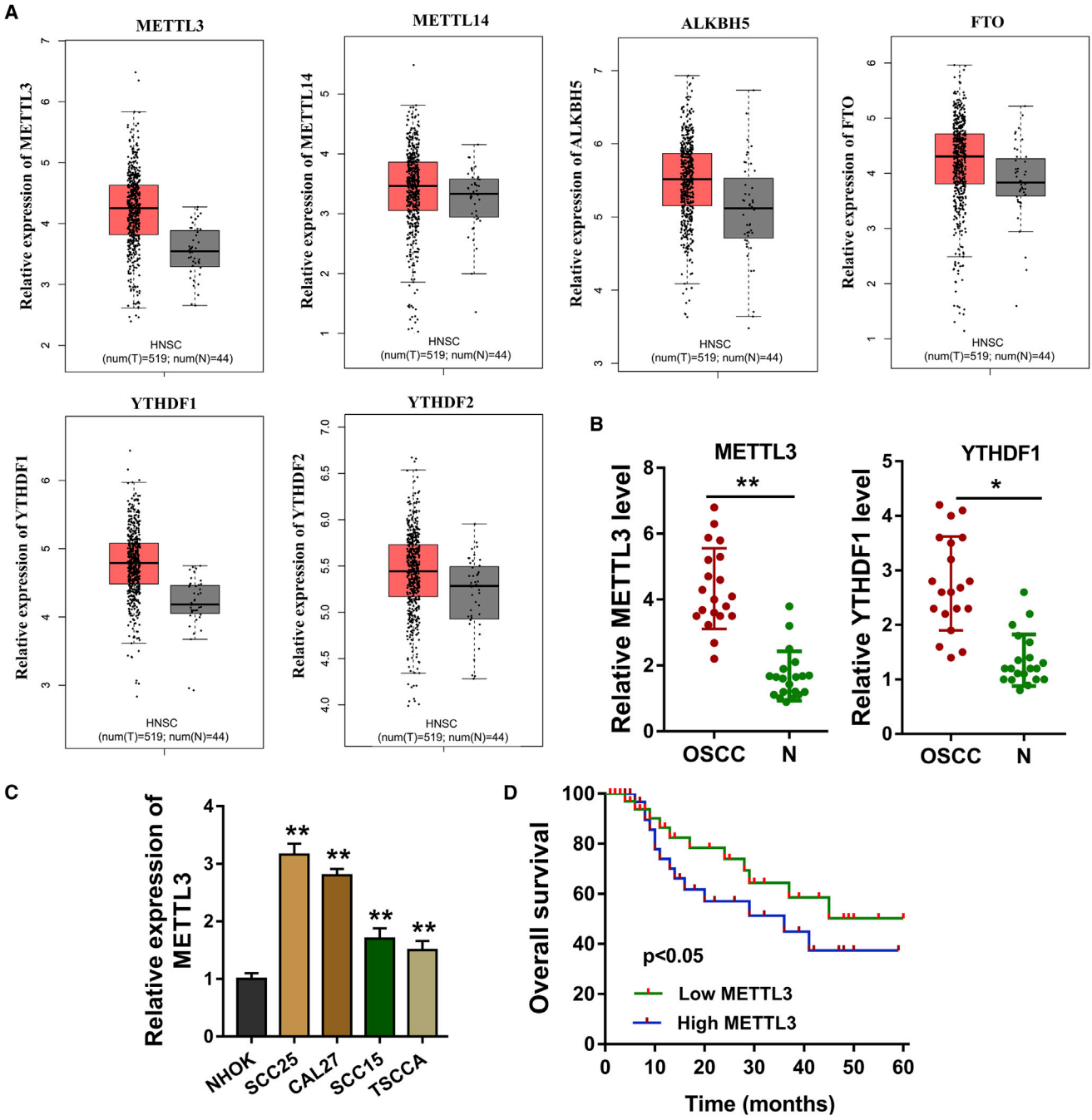

Figure 2. m^{6}A Methyltransferase METTL3 Indicates the Poor Prognosis of OSCC

(A) Results based on the TCGA (http://software.broadinstitute.org/software/igv/tcga) and GEPIA (http://gepia.cancer-pku.cn/index.html) databases showed the expression level of methyltransferase (METTL3, METTL14), demethyltransferase (ALKBH5, FTO), and reader (YTHDF1, YTHDF2). (B) qRT-PCR illustrated the quantitative analysis of METTL3 and YTHDF1. (C) In the OSCC cells, quantitative analysis of METTL3 was performed by the qRT-PCR. (D) Kaplan-Meier and log-rank testing showed the prognosis of patients in the OSCC patients cohort. Three independent experiments were performed. *$p < 0.05$ versus control; **$p < 0.01$ versus control.

In present study, we herein identified that METTL3, a major RNA N^6-adenosine methyltransferase, was significantly upregulated in human OSCC tissue and cells. Knockdown of METTL3 remarkably repressed the proliferation, invasion, and migration *in vitro* and tumorigenicity *in vivo*. In further research, we identify the m^{6}A-increased c-Myc stability mediated by YTHDF1. The METTL3/m^{6}A/YTHDF1/c-Myc axis might provide a novel insight for OSCC-targeted therapy.

Table 1. Correlation within METTL3 Expression and the Clinicopathological Characteristic of OSCC Patients

		METTL3 Expression		
Characteristics	T = 20	Low (9)	High (11)	p Value
Gender				
Male	12	6	6	0.475
Female	8	3	5	
Age				
<60 years	11	5	6	0.725
≥60 years	9	4	5	
TNM Stage				
I–II	6	3	3	0.025[a]
III–IV	14	6	8	
Tumor Size				
<3 cm	7	3	4	0.322
≥3 cm	13	6	7	
Histological Differentiation				
Well/moderate	11	6	5	0.468
Poor	9	3	6	

TNM, Tumor-Node-Metastasis.
[a]$p < 0.05$ represents statistical differences.

RESULTS

MeRIP-Seq Analysis Unveils the m^{6}A Profiles in OSCC Cells

To investigate the downstream target mRNAs of METTL3, m^{6}A-RNA immunoprecipitation sequencing (MeRIP-seq) was performed using OSCC cells and normal cells to analyze the potential m^{6}A site distributions in the target mRNAs. A proportion of m^{6}A peak distributions displayed the m^{6}A peaks in the 3′ untranslated region (UTR), 5′ UTR, exon, intron, downstream region, and distal intergenic region (Figure 1A). The metagene profile of m^{6}A distribution showed that the m^{6}A peaks were primarily enriched around the stop codon, including coding sequences (CDSs) and 3′ UTRs (Figure 1B). Pathway analysis showed the potential pathway for OSCC (Figure 1C). Gene Ontology (GO) analysis showed the target manners for OSCC (Figure 1D). The volcano plot for MeRIP-seq analysis showed the different expression of transcripts, including upregulated and downregulated transcripts (Figure 1E). The Integrative Genomics Viewer (IGV) tool revealed the m^{6}A peak distribution c-Myc mRNA (Figure 1F).

m^{6}A Methyltransferase METTL3 Indicates the Poor Prognosis of OSCC

Our team focused on the roles of m^{6}A modification on OSCC tumorigenesis, and then we investigated the critical elements in this regulation, including methyltransferase (METTL3, METTL14), demethyltransferase (ALKBH5, FTO), and reader (YTHDF1, YTHDF2). Results based on the The Cancer Genome Atlas (TCGA; http://software.broadinstitute.org/software/igv/tcga) and Gene Expression Profiling Interactive Analysis (GEPIA; http://gepia.cancer-pku.cn/index.html) databases showed that the expression levels of m^{6}A catalytic proteins were upregulated in varying degrees, including METTL3, METTL14, ALKBH5, FTO, YTHDF1, and YTHDF2 (Figure 2A). In our enrolled OSCC tissue specimens, quantitative analysis found that METTL3 and YTHDF1 were upregulated (Figure 2B). In OSCC cells, the level of METTL3 was upregulated compared with the control normal cells (Figure 2C). In the OSCC patients' cohort, the high expression of METTL3 indicated the poor prognosis of OSCC patients (Figure 2D; Table 1). Clinically, m^{6}A methyltransferase METTL3 indicates the poor prognosis of OSCC.

METTL3 Accelerates the Proliferation, Invasion, and Migration of OSCC Cells

To investigate the biological roles of METTL3 for OSCC cells, we established METTL3 silencing or overexpression via the stable transfection into SCC25 cells and CAL27 cells. Quantitative real-time reverse transcription polymerase chain reaction (qRT-PCR) analysis showed that METTL3 mRNA was significantly reduced in SCC25 cells, whereas it was remarkably upregulated in the CAL27 cells (Figure 3A). Then, gain- and loss-of-functional assays were performed to identify the roles of METTL3 in OSCC cells (SCC25, CAL27). Western blot analysis showed that METTL3 short hairpin RNA (shRNA) silenced its protein expression, and METTL3 overexpression plasmids enhanced its protein level (Figure 3B). For the proliferation ability, 5-ethynyl-2′-deoxyuridine (EdU) assay was performed and illustrated that METTL3 promoted the proliferation of OSCC cells (Figure 3C). Wound-healing assay illustrated that METTL3 promoted the migration of OSCC cells (Figure 3D). Transwell invasion and migration assay elucidated that METTL3 silencing repressed the invasion and migration, whereas METTL3 overexpression promoted the invasion and migration (Figures 3E and 3F). Therefore, these evidences support that METTL3 accelerates the proliferation, invasion, and migration of OSCC cells.

METTL3 Catalyzes the c-Myc mRNA 3′ UTR Methylation to Facilitate Its Stability

Our previous research has reported the critical roles of oncogene c-Myc in OSCC tumorigenesis.[22] Moreover, Vu et al.[23] indicated that METLL3 could facilitate the translation of c-Myc in myeloid leukemia, which inspired us to reveal whether METTL3 could regulate the expression of c-Myc. The consensus motif of METTL3 was identified (GGACU) in the m^{6}A modification targeting the 3′ UTR of c-Myc mRNA, which was adjacent to the stop codon (Figures 4A and 4B). The GEPIA database derived by TCGA illustrated that c-Myc expression was positively correlated with METTL3 in head and neck cancer individuals (Figure 4C). Dot blot analysis (Figure 4D) and m^{6}A quantitative analysis (Figure 4E) showed that METTL3 silencing reduced the global m^{6}A modification level, whereas METTL3 overexpression accelerated the level in OSCC cells (SCC25, CAL27). RNA immunoprecipitation following qPCR (RIP-qPCR) showed that the METTL3 directly interacted with c-Myc mRNA (Figure 4F). Western blot analysis indicated that METTL3 silencing reduced c-Myc protein expression, whereas METTL3 overexpression enhanced it (Figure 4G). The RNA stability assay showed that the mRNA half-life ($t_{1/2}$) was shortened by METTL3 silencing, which was prolonged by METTL3 overexpression

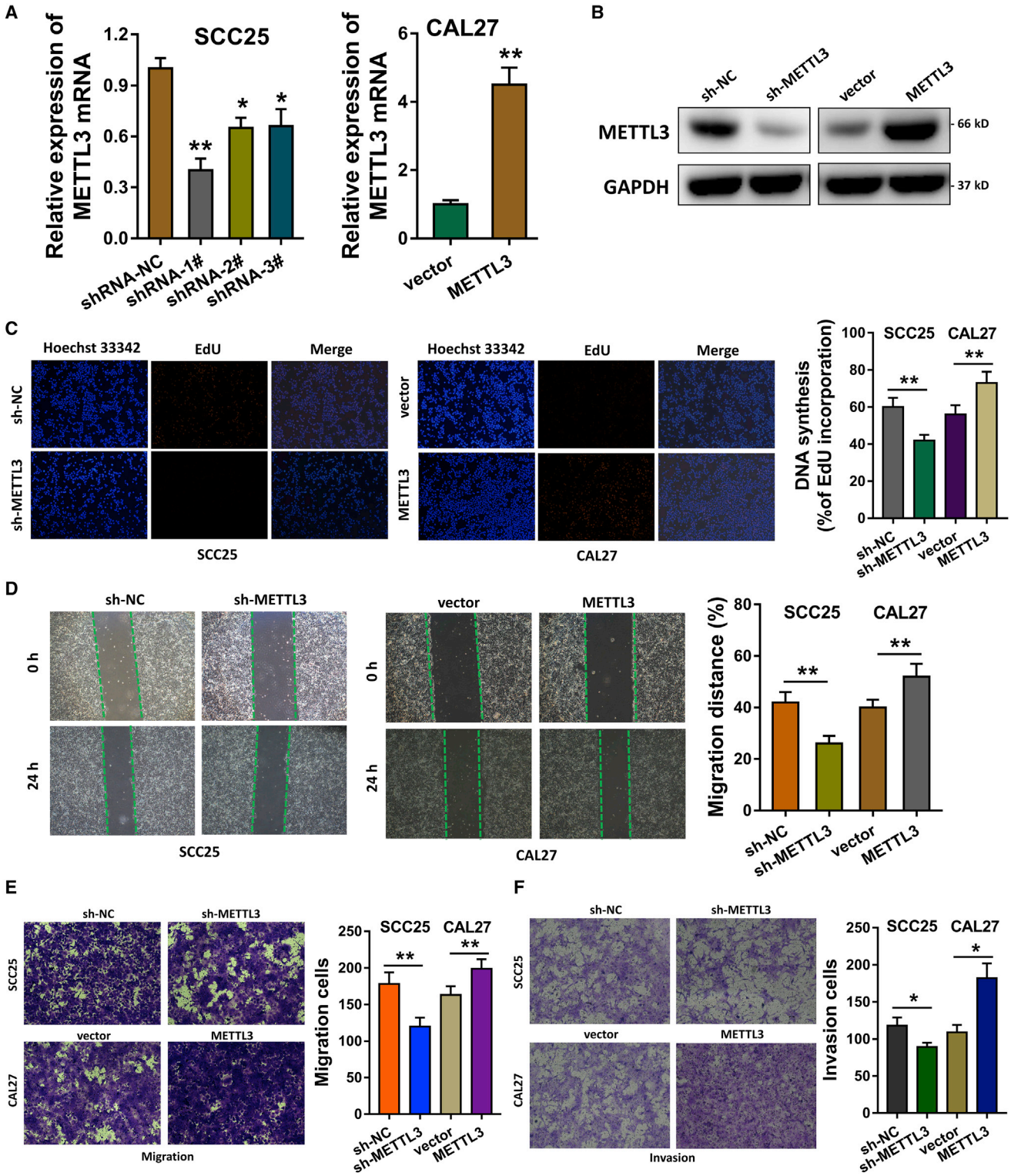

Figure 3. METTL3 Accelerates the Proliferation, Invasion, and Migration of OSCC Cells

(A) Plasmids of METTL3 silencing or overexpression were transfected to establish the stable transfection in SCC25 cells and CAL27 cells. qRT-PCR analysis detected the METTL3 mRNA expression. (B) Western blot analysis showed the protein levels of METTL3 in SCC25 and CAL27 cells transfected with METTL3

(legend continued on next page)

(Figure 4H). Overall, these findings illustrate that METTL3 mediates the c-Myc mRNA 3′ UTR methylation to enhance its mRNA stability.

YTHDF1 Mediates the c-Myc Stability through an m^{6}A-Dependent Manner

In the previous research, METTL3 could activate the targets' transcripts' stability via a YTHDF1-mediated m^{6}A-dependent manner. Therefore, we wonder whether YTHDF1 participated in c-Myc transcript expression facilitated by METTL3 in OSCC cells. In the public database (GEPIA), we found that the expression of YTHDF1 was positively correlated with that of c-Myc (Figure 5A). Western blot analysis showed that YTHDF1 silencing could repress c-Myc protein expression, whereas YTHDF1 overexpression could enhance c-Myc protein expression (Figure 5B), indicating that YTHDF1 could promote c-Myc expression. RIP-qPCR illustrated that YTHDF1 could directly interact with c-Myc mRNA, indicating the potential targeting of YTHDF1 on c-Myc mRNA (Figure 5C). The RNA stability assay showed that the mRNA $t_{1/2}$ was shortened by YTHDF1 silencing, which was prolonged by YTHDF1 overexpression (Figure 5D). RIP-qPCR unveiled that METTL3 inhibition could impair the direct interaction within YTHDF1 and c-Myc mRNA in OSCC cells, indicating the close connection within METTL3, YTHDF1, and c-Myc mRNA (Figure 5E). In conclusion, these data evidence that YTHDF1 mediates c-Myc stability through an m^{6}A-dependent manner.

Knockdown of METTL3 Represses OSCC Tumor Growth *In Vivo*

Given the oncogenic role of METTL3 for OSCC cells identified in previous finding in *vitro*, in order to investigate the biological role of METTL3 on OSCC tumor growth, the stable transfection of METTL3 silencing was performed using SCC25 cells (Figure 6A). Results elucidated that knockdown of METTL3 significantly repressed the tumor growth (volume and weight) compared to the blank control groups (Figures 6B and 6C). Hematoxylin and eosin (H&E) staining and immunohistochemical (IHC) staining illustrated that METTL3 knockdown reduced the OSCC tumor process and c-Myc abundance (Figure 6D). In conclusion, these findings unravel that knockdown of METTL3 represses OSCC tumor growth *in vivo*.

DISCUSSION

To date, accumulating literature indicate the essential roles of m^{6}A in human diseases, especially multiple cancers.[24] The epigenetic regulation for OSCC is increasingly critical, including noncoding RNA, histone modification, and DNA methylation.[25–27] However, the regulation of m^{6}A modification in OSCC is still unclear. In the past several years, there are three major m^{6}A regulators, including methyltransferase (writers), demethylase (erasers), and methylation recognition (reader) enzymes. Regarding the methyltransferase, METTL3 acts as the most widely recognized enzyme in which its roles have been investigated in human cancers.

In our research, we found that there are several m^{6}A key enzymes upregulated in OSCC tissue samples, especially the METTL3, ALKBH5, and YTHDF1. One drawback in this clinical evidence is that the sample size is limited. However, to a certain extent, these findings inspire us that the m^{6}A might participate in OSCC tumorigenesis. Besides, the ectopic overexpression of METTL3 indicated the poor clinical outcome of OSCC patients. In further research, we focused on the roles of METTL3, the well-known methyltransferase, in OSCC and unveiled the potential mechanism involved in this pathological process. *In vitro* cellular experiments, gain- and loss-of-functional assay, illustrated that METTL3 could accelerate OSCC proliferation, migration, and invasion, indicating that METTL3 might act as an oncogene in OSCC tumorigenesis.

METTL3 could install the eukaryotic messenger RNA methylation on the N^6 nitrogen of adenosine. The similar m^{6}A installation that METTL3 catalyzes is also motivated by METTL14 and WTAP. Once the mRNA is installed with methyl, the biological characteristics of mRNA were varied. For example, the CDS regions of SOX2 transcripts were methylated by METTL3 through the IGF2BP2 to prevent SOX2 mRNA degradation.[28] In gastric cancer, METTL3 interacted with SEC62 and induced the m^{6}A on SEC62 mRNA, therefore promoting the stabilizing of SEC62 mRNA via IGF2BP1.[29] Therefore, in this m^{6}A regulation event, METTL3 could install the m^{6}A on mRNA and enhance the stability.

In the present work, MeRIP-seq identified that the m^{6}A peaks were significantly enriched in the surrounding region of the stop codon, including the CDS and 3′ UTR region. Accurately, the m^{6}A sites of c-Myc transcript are located into the 3′ UTR region. The consensus motif (GGACU) of the 3′ UTR region of the c-Myc transcript is near to the stop codon (TAA or UAA), which is consistent with the MeRIP-seq analysis. In further investigations, we confirmed that METTL3 could upregulate the methylation level and promote the stability of the c-Myc mRNA. c-Myc acts as an essential oncogenic factor in human cancer.[30,31] Previous literature inspired that m^{6}A readers (YTHDF1) might participate in the target transcript's stability; therefore, we focus on the possible roles of METTL3 and YTHDF1 in c-Myc stability. As expected, results confirmed that METTL3 enhanced c-Myc mRNA stability via a YTHDF1-mediated m^{6}A manner (Figure 7).

Given that METTL3 could install the m^{6}A modification of its target transcript, the fortunes of these mRNA are different depending on the reader's recognition mode. For example, METTL3 augments the m^{6}A modification in Snail CDS but not 3′ UTR, triggering polysome-mediated translation of Snail mRNA in liver cancer cells, and this promotion is mediated by YTHDF1 on Snail mRNA.[32] However, the m^{6}A installed by METTL3 could mediate the degradation of target mRNA. For example, suppressor of

shRNA or overexpression plasmids. (C) EdU assay was performed to illustrate the proliferation ability of OSCC cells. (D) Wound-healing assay illustrated the migration of OSCC cells. (E) Transwell assay elucidated the migration of OSCC cells in SCC25 and CAL27 cells transfected with METTL3 shRNA or overexpression plasmids. (F) Transwell assay elucidated the invasion of OSCC cells. Three independent experiments were performed. *$p < 0.05$ versus control; **$p < 0.01$ versus control.

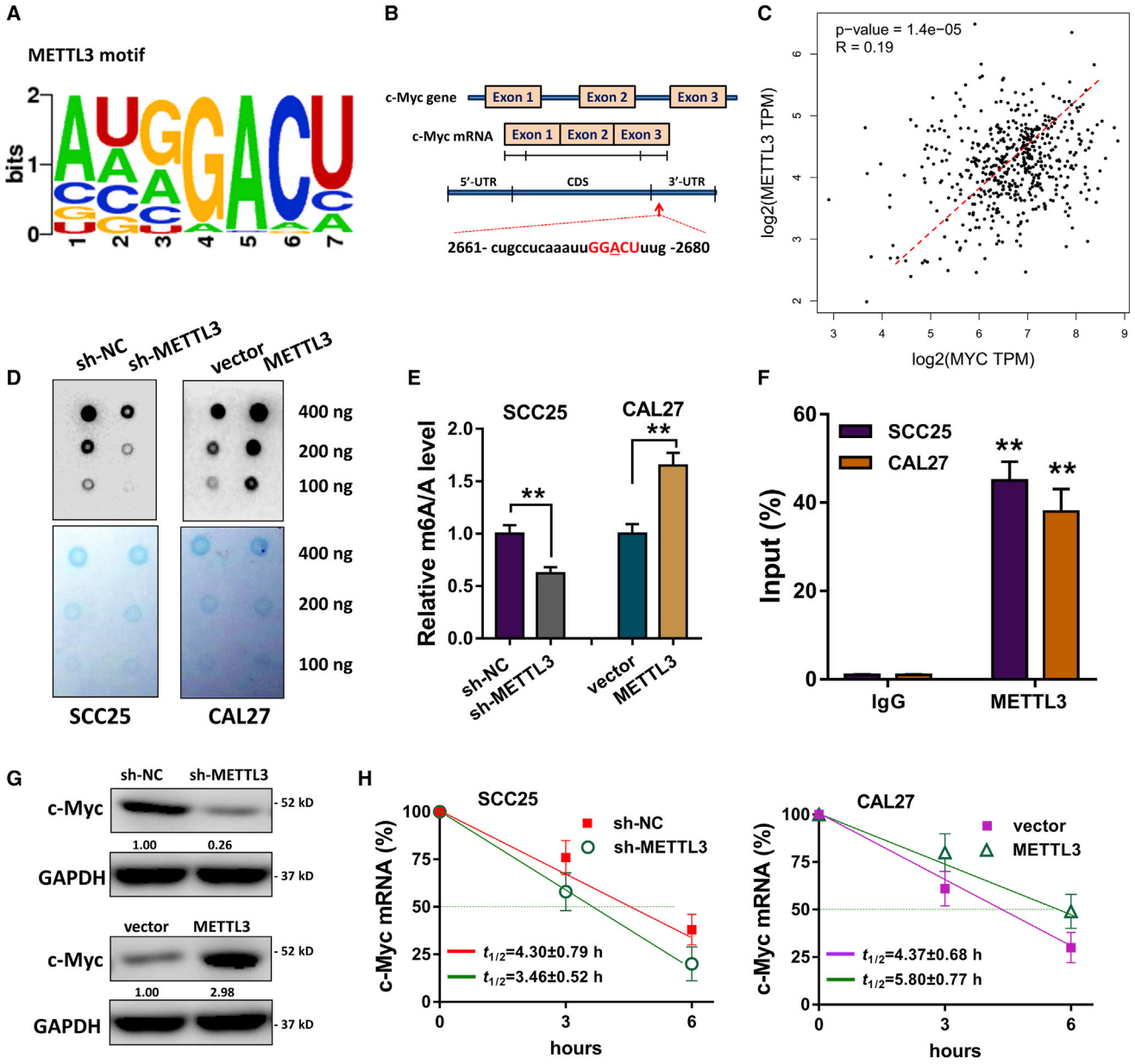

Figure 4. METTL3 Catalyzes the c-Myc mRNA 3′ UTR Methylation to Enhance Its mRNA Stability

(A) The consensus motif of METTL3 (GGACU) targeting the 3′ UTR of c-Myc mRNA m^{6}A modification. (B) The location of the m^{6}A site in the c-Myc mRNA. (C) GEPIA database derived by TCGA illustrated the correlation within c-Myc and METTL3 expression. (D and E) Dot blot analysis (D) and m^{6}A quantitative analysis (E) were performed for the global m^{6}A modification level. (F) RNA immunoprecipitation following qPCR (RIP-qPCR) showed the interaction within METTL3 protein and c-Myc mRNA. (G) Western blot analysis indicated the c-Myc protein expression. (H) RNA stability assay showed the mRNA half-life ($t_{1/2}$) with the METTL3 silencing or METTL3 overexpression transfection. Three independent experiments were performed. **p < 0.01 versus control.

cytokine signaling 2 (SOCS2), a target of METTL3-mediated m^{6}A modification, is repressed by METTL3 through an m^{6}A-YTHDF2-dependent mechanism in hepatocellular carcinoma (HCC).[33] Overall, we could conclude the bidirectional functions of METTL3 in human cancer oncogenesis mediated by different downstream recognition and mediating mechanisms.

Conclusion

In conclusion, our findings confirm the oncogenic role of METTL3 in OSCC tumorigenesis. We herein identify the m^{6}A-increased c-Myc stability mediated by YTHDF1. The METTL3/m^{6}A/YTHDF1/c-Myc axis might provide novel insight for OSCC-targeted therapy.

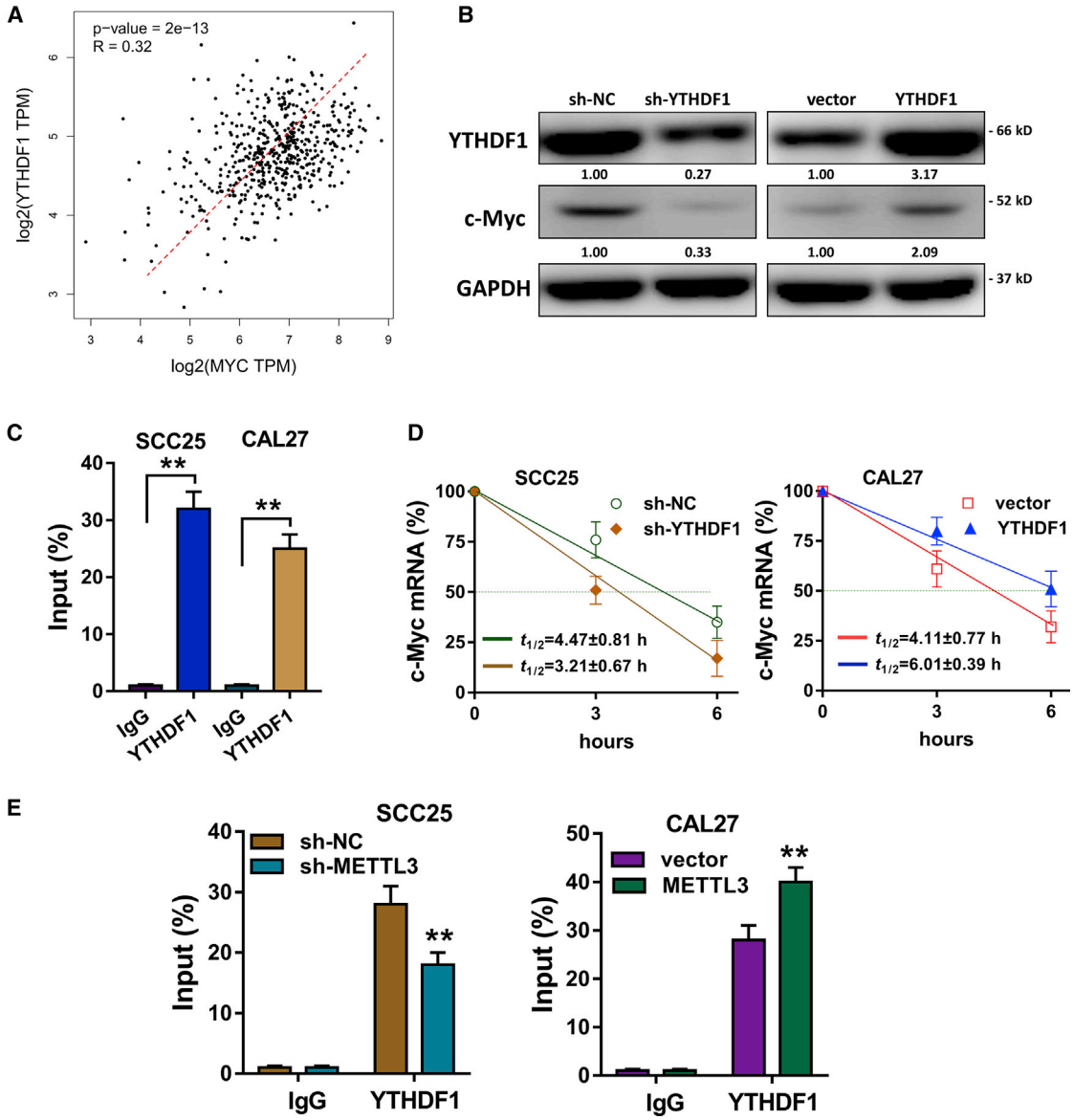

Figure 5. YTHDF1 Mediates the c-Myc Stability through an m^{6}A-Dependent Manner

(A) In the public database (GEPIA), the expression of YTHDF1 was positively correlated with that of c-Myc. (B) Western blot analysis showed the c-Myc protein expression in SCC25 and CAL27 cells transfected with YTHDF1 silencing or YTHDF1 overexpression. (C) RNA immunoprecipitation following qPCR (RIP-qPCR) illustrated the direct interaction of YTHDF1 targeting c-Myc mRNA. (D) After actinomycin D (Act-D; 5 μg/mL), RNA stability assay showed the mRNA half-life ($t_{1/2}$) of SCC25 and CAL27 cells transfected with YTHDF1 silencing or YTHDF1 overexpression. (E) RIP-qPCR unveiled the interaction within YTHDF1 and c-Myc mRNA after METTL3 inhibition. Three independent experiments were performed. **$p < 0.01$ versus control.

MATERIALS AND METHODS

Clinical Samples

OSCC tissue specimens and matched nontumorous tissue were excised during the surgery and stored at −80°C for further extraction and analysis. After the surgery, the pathological classification was carried by two pathologists. The processes were performed according to the principles of the Declaration of Helsinki. The clinical human research had been approved by the Institutional Ethics Committee of The Hospital of Stomatology Tianjin Medical University.

Cell Culture

The OSCC cell lines (SCC25, CAL27, SCC15, TSCCA) were provided by ATCC (American Type Culture Collection; Manassas, VA, USA), and normal oral keratinocytes (NHOKs) were provided by the Institute of Biochemistry and Cell Biology of the Chinese Academy of

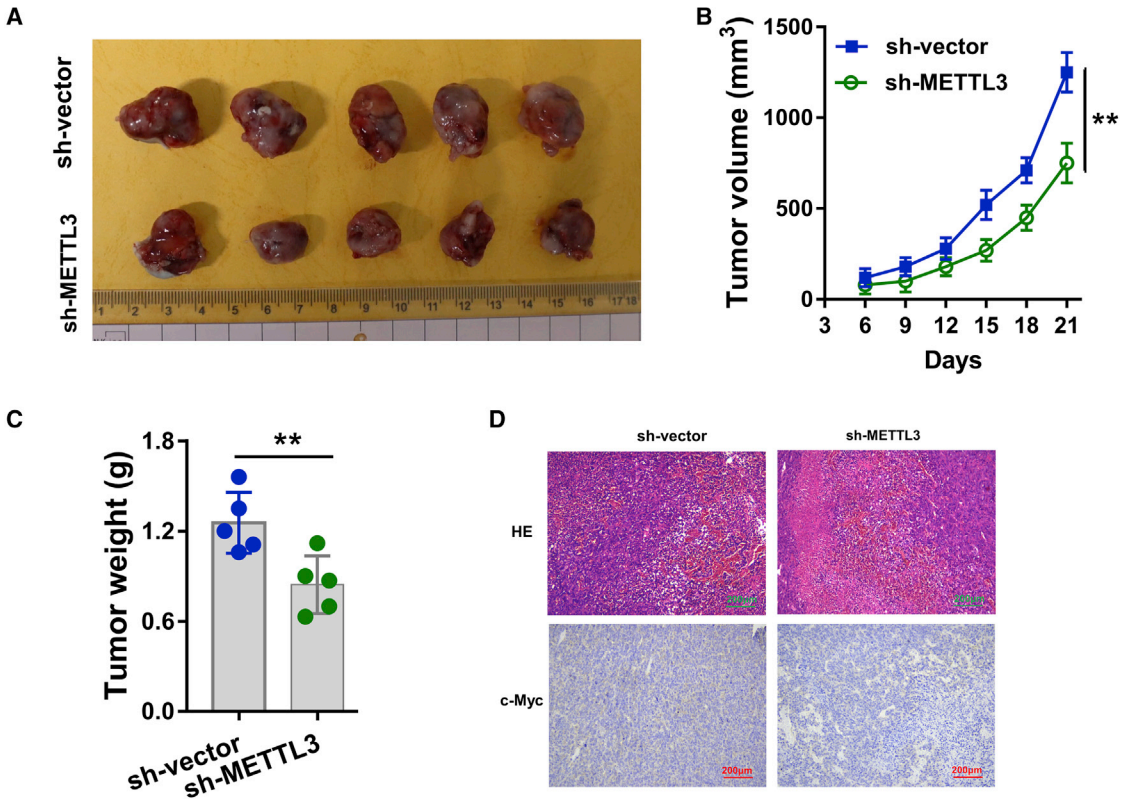

Figure 6. Knockdown of METTL3 Represses the OSCC Tumor Growth In Vivo

(A) An *in vivo* xenograft assay was performed using the SCC25 cells transfected with METTL3 stable silencing (sh-METTL3) or controls (sh-vector). (B and C) The tumor growth (volume in B and weight in C) was detected in METTL3 knockdown transfection as compared to the blank control groups. (D) Hematoxylin and eosin (HE) staining and immunohistochemical (IHC) staining illustrated the c-Myc abundance in neoplasm. Three independent experiments were performed. $^{**}p < 0.01$ versus control.

Sciences (Shanghai, China). Cells were cultured in DMEM (Dulbecco's modified Eagle's medium; Gibco, Carlsbad, CA, USA) medium containing 10% fetal bovine serum (FBS) and 100 U/mL penicillin and 100 mg/mL streptomycin.

shRNA and Overexpression of Plasmid Transfection

The shRNAs and overexpression plasmids targeting METTL3 and YTHDF1 were synthesized. For the stable silencing, shRNA lentivirus (lenti-sh-METTL3, lenti-sh-YTHDF1) were constructed using pLKD-CMV-EGFP vectors. For overexpression, cDNA was PCR amplified and subcloned into the pcDNA3.1 vector (Invitrogen), according to the manufacturer's instructions. After transfection, the expression of METTL3 and YTHDF1 was validated by qPCR analysis and western blot.

Total RNA Extraction and qRT-PCR

Total cellular RNA was extracted from the OSCC tissue and cells with TRIzol (Invitrogen), according to the manufacturer's instructions. RNA was quantified using a Nanodrop (ND-100; Nanodrop Technologies, Wilmington, DE, USA), according to a 260/280-nm ratio. cDNA was prepared using the SuperScript First-Stand Synthesis system (Invitrogen, USA). qPCR was performed utilizing the ABI PRISM 7500 sequence detection system (Applied Biosystems, Foster City, CA, USA), and SYBR Green fluorescence was detected by iQ SYBR Green Supermix (Applied Biosystems, Carlsbad, CA, USA). Relative quantitation of these data was calculated from the $2^{-\Delta\Delta Ct}$ method normalized to glyceraldehyde 3-phosphate dehydrogenase (GAPDH) from triplicate data. The primers for the PCR analysis were listed in Table S1.

Western Blot Analysis

Cells were lysed using radioimmunoprecipitation assay (RIPA) buffer (Beyotime, Shanghai, China), supplementing with protease inhibitor. Protein concentration was detected using a bicinchoninic acid (BCA) protein assay kit (Thermo Fisher Scientific, MA, USA). The lysed protein extract was subjected to 10% SDS-PAGE and was transferred to a polyvinylidene fluoride (PVDF) membrane (Millipore, Billerica, MA, USA) and then blocked with 5% nonfat milk. Membranes were incubated with the primary antibodies (Abcam, Cambridge, MA, USA) overnight at 4°C and with anti-METTL3 (Abcam; ab195352, 1:1,000), anti-YTHDF1 antibody (Abcam; ab220162, 1:1,000), and anti-c-Myc antibody (Abcam; ab56, 1:1,000). Then, the members were conjugated to horseradish peroxidase (HRP) for 2 h at room temperature as controls. Finally, the blots were detected by using

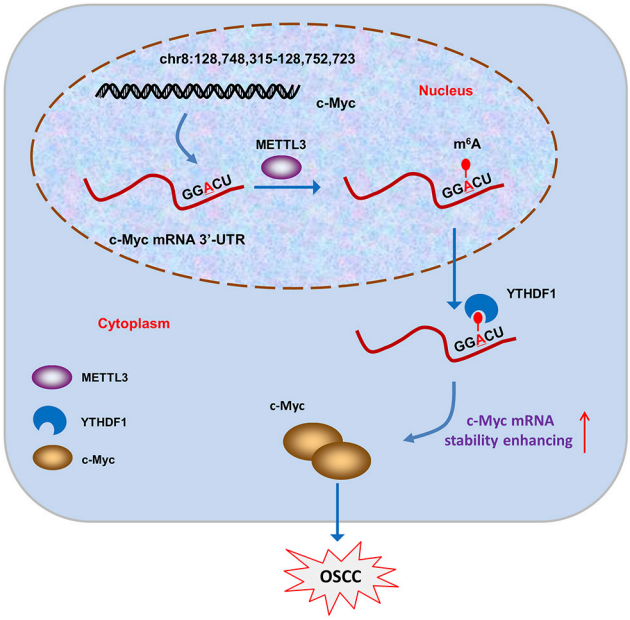

Figure 7. METTL3 Enhanced the c-Myc Stability via a YTHDF1-Mediated m^{6}A Manner

enhanced chemiluminescence (ECL) detection reagent (Thermo Fisher Scientific).

EdU Incorporation and Wound-Healing Assay

The proliferation potential of OSCC cells was detected using EdU and a wound-healing assay. For the EdU, the transfected OSCC cells (SCC25, CAL27) were administrated using EdU Apollo DNA *in vitro* kit (Ribobio, Guangzhou, China), following the manufacturer's instructions. The DNA synthesis rate was measured under an immunofluorescence microscope. For the wound-healing assay, OSCC cells were seeded into the six-well plates at about 90% confluence. After the medium was removed, the monolayer was manually wounded by a 200-μL pipette tip. The wounding scratch width was measured at different time points and calculated as relative percentage of the initial distance (0 h, 100%).

Transwell Assay

A transwell assay was performed for the invasion and transwell analysis. In brief, SCC25 and CAL27 cells were harvested and seeded to the upper transwell chamber (5×10^4) into an 8-mm pore transwell plate preapplied with 50 μL Matrigel or not. Serum-free medium (200 μL) was added onto the upper chamber, and the medium (600 μL) containing 20% FBS was added into the lower chamber. Following 24 h incubation, the unmigrated or uninvaded cells were cleaned using a cotton swab and then fixed in 4% paraformaldehyde for 20 min and stained with hematoxylin. Images were taken, and the cell number was calculated.

Dot Blot Assay

Dot blots were performed as previously described.[34] Cellular total RNA was isolated, and the mRNA concentration was measured by NanoDrop. Then, the isolated RNA (400 ng) was spotted onto a nylon membrane (GE Healthcare) and then crosslinked by UV irradiation. The nylon membrane was incubated with m^{6}A antibody (Abcam; ab208577, 1:100) overnight at 4°C. The dot blots were visualized by Immobilon Western Chemiluminscent HRP Substrate (Merck Millipore, Germany). For the control, an equal amount of RNAs (400 ng) was spotted on the nylon membrane and then stained with 0.02% methylene blue in 0.3 M sodium acetate (pH 5.2) for 2 h followed with ribonuclease-free water washing for about 5 h.

MeRIP-Seq and RIP-qPCR

Me-RIP was performed as previously described.[33] Total RNA was extracted from the SCC25 cells and then immunoprecipitated with m^{6}A antibody (Abcam; ab151230) using Magna Me-RIP m^{6}A Kit (Merck Millipore), according to the manufacturer's protocols. After immunoprecipitation, part of the RNA was analyzed using high-throughput sequencing by Jiayin Biotechnology (Shanghai, China), and part of RNA was calculated using quantitative RT-PCR for quantitative analysis.

Quantification of the m^{6}A Modification

From OSCC cells, the total RNA was isolated using TRIzol (Invitrogen), according to the manufacturer's instruction. Briefly, RNA (200 ng) was incubated with capture antibody solution in a suitable diluted concentration. The global m^{6}A level of mRNA was measured by an m^{6}A -RNA methylation quantification kit (Abcam; ab185912), following the manufacturer's protocol. The m^{6}A levels colorimetrically were quantified by reading the absorbance at a wavelength of 450 nm.

RNA Stability

To detect the RNA stability in SCC25 and CAL27 cells, actinomycin D (Act-D; 5 μg/mL; Sigma, USA) was administrated to cells. At the indicated time point, RNA was isolated using TRIzol reagent (Invitrogen, Grand Island, NY, USA) and analyzed by real-time PCR, normalized to GAPDH. $t_{1/2}$ of mRNA was calculated.

In Vivo Xenograft Mice Assay

Male BALB/c nude mice (4–5 weeks old, 10 mice) were provided by SPF Laboratory Technology (Beijing, China) and raised under specific pathogen-free conditions. The stable transfection of SCC25 cells (1×10^7 cells in 0.1 mL) with lenti-sh-METTL3 or blank vectors was injected subcutaneously into BALB/c nude mice. Tumor width and length were recorded every 3 days by the following formula: volume = (length × width^2)/2. The tumor weight was detected after the mice were sacrificed. The animal experiment was approved by the Ethics Committee of The Hospital of Stomatology, Tianjin Medical University.

Statistical Analysis

Statistical tests were performed using SPSS version 19.0 for Windows (SPSS, Chicago, IL, USA) and GraphPad version 7.0 Prism (GraphPad Software, La Jolla, CA, USA). A continuous variable was presented as the mean ± standard deviations or standard errors. For matched group analysis, the significant differences were analyzed

via Student's unpaired t test. For multiple groups, the significant differences were analyzed by one-way ANOVA, followed by Tukey's honest testing. Survival curves were assessed by the Kaplan-Meier and log-rank testing. A p value less than 0.05 was considered to be statistically significant.

SUPPLEMENTAL INFORMATION

Supplemental Information can be found online at https://doi.org/10.1016/j.omtn.2020.01.033.

AUTHOR CONTRIBUTIONS

W.Z., Y.C., and L.L. performed the experiments and wrote the paper. X.Q., X.M., Y.W., Z.L., and S.M. acted as the assistants. J.W. and J.L. are responsible for the design and for funding collection. All authors read and approved the final manuscript.

CONFLICTS OF INTEREST

The authors declare no competing interests.

ACKNOWLEDGMENTS

This work was supported by National Natural Science Foundation of China (grant/award number: 81701019), Tianjin Science and Technology Commission General Project (grant/award number: 18JCYBJC92400), Tianjin Stomatology Hospital Doctor/Master Key Project (grant/award number: 2019BSZD06) and Tianjin Science and Technology Commission General Project (grant/award number: 20JCYBJC00000, Jingwen Liu).

REFERENCES

1. Moharil, R.B., Dive, A., Khandekar, S., and Bodhade, A. (2017). Cancer stem cells: An insight. J. Oral Maxillofac. Pathol. *21*, 463.

2. Dumache, R. (2017). Early Diagnosis of Oral Squamous Cell Carcinoma by Salivary microRNAs. Clin. Lab. *63*, 1771–1776.

3. Martins, F., Mistro, F.Z., Kignel, S., Palmieri, M., do Canto, A.M., and Braz-Silva, P.H. (2017). Pigmented Squamous Cell Carcinoma In Situ: Report of a New Case and Review of the Literature. J. Clin. Exp. Dent. *9*, e1362–e1365.

4. Lakshminarayana, S., Augustine, D., Rao, R.S., Patil, S., Awan, K.H., Venkatesiah, S.S., Haragannavar, V.C., Nambiar, S., and Prasad, K. (2018). Molecular pathways of oral cancer that predict prognosis and survival: A systematic review. J. Carcinog. *17*, 7.

5. Farag, A.F., Abou-Alnour, D.A., and Abu-Taleb, N.S. (2018). Oral carcinoma cuniculatum, an unacquainted variant of oral squamous cell carcinoma: A systematic review. Imaging Sci. Dent. *48*, 233–244.

6. Chen, J., Fang, X., Zhong, P., Song, Z., and Hu, X. (2019). N6-methyladenosine modifications: interactions with novel RNA-binding proteins and roles in signal transduction. RNA Biol. *16*, 991–1000.

7. Ianniello, Z., Paiardini, A., and Fatica, A. (2019). N^6-Methyladenosine (m^6A): A Promising New Molecular Target in Acute Myeloid Leukemia. Front. Oncol. *9*, 251.

8. Li, Y., Wang, X., Li, C., Hu, S., Yu, J., and Song, S. (2014). Transcriptome-wide N^6-methyladenosine profiling of rice callus and leaf reveals the presence of tissue-specific competitors involved in selective mRNA modification. RNA Biol. *11*, 1180–1188.

9. Luo, G.Z., MacQueen, A., Zheng, G., Duan, H., Dore, L.C., Lu, Z., Liu, J., Chen, K., Jia, G., Bergelson, J., and He, C. (2014). Unique features of the m6A methylome in Arabidopsis thaliana. Nat. Commun. *5*, 5630.

10. Garcia-Campos, M.A., Edelheit, S., Toth, U., Safra, M., Shachar, R., Viukov, S., Winkler, R., Nir, R., Lasman, L., Brandis, A., et al. (2019). Deciphering the "m^6A Code" via Antibody-Independent Quantitative Profiling. Cell *178*, 731–747.e16.

11. Linder, B., Grozhik, A.V., Olarerin-George, A.O., Meydan, C., Mason, C.E., and Jaffrey, S.R. (2015). Single-nucleotide-resolution mapping of m6A and m6Am throughout the transcriptome. Nat. Methods *12*, 767–772.

12. Zhao, W., Qi, X., Liu, L., Liu, Z., Ma, S., and Wu, J. (2019). Epigenetic Regulation of m^6A Modifications in Human Cancer. Mol. Ther. Nucleic Acids *19*, 405–412.

13. Lan, Q., Liu, P.Y., Haase, J., Bell, J.L., Hüttelmaier, S., and Liu, T. (2019). The Critical Role of RNA m^6A Methylation in Cancer. Cancer Res. *79*, 1285–1292.

14. Song, H., Feng, X., Zhang, H., Luo, Y., Huang, J., Lin, M., Jin, J., Ding, X., Wu, S., Huang, H., et al. (2019). METTL3 and ALKBH5 oppositely regulate m^6A modification of *TFEB* mRNA, which dictates the fate of hypoxia/reoxygenation-treated cardiomyocytes. Autophagy *15*, 1419–1437.

15. Cheng, M., Sheng, L., Gao, Q., Xiong, Q., Zhang, H., Wu, M., Liang, Y., Zhu, F., Zhang, Y., Zhang, X., et al. (2019). The m^6A methyltransferase METTL3 promotes bladder cancer progression via AFF4/NF-κB/MYC signaling network. Oncogene *38*, 3667–3680.

16. Liu, J., Eckert, M.A., Harada, B.T., Liu, S.M., Lu, Z., Yu, K., Tienda, S.M., Chryplewicz, A., Zhu, A.C., Yang, Y., et al. (2018). m^6A mRNA methylation regulates AKT activity to promote the proliferation and tumorigenicity of endometrial cancer. Nat. Cell Biol. *20*, 1074–1083.

17. Selberg, S., Blokhina, D., Aatonen, M., Koivisto, P., Siltanen, A., Mervaala, E., Kankuri, E., and Karelson, M. (2019). Discovery of Small Molecules that Activate RNA Methylation through Cooperative Binding to the METTL3-14-WTAP Complex Active Site. Cell Rep. *26*, 3762–3771.e5.

18. Barbieri, I., Tzelepis, K., Pandolfini, L., Shi, J., Millán-Zambrano, G., Robson, S.C., Aspris, D., Migliori, V., Bannister, A.J., Han, N., et al. (2017). Promoter-bound METTL3 maintains myeloid leukaemia by m^6A-dependent translation control. Nature *552*, 126–131.

19. Yue, B., Song, C., Yang, L., Cui, R., Cheng, X., Zhang, Z., and Zhao, G. (2019). METTL3-mediated N6-methyladenosine modification is critical for epithelial-mesenchymal transition and metastasis of gastric cancer. Mol. Cancer *18*, 142.

20. Niu, Y., Lin, Z., Wan, A., Chen, H., Liang, H., Sun, L., Wang, Y., Li, X., Xiong, X.F., Wei, B., et al. (2019). RNA N6-methyladenosine demethylase FTO promotes breast tumor progression through inhibiting BNIP3. Mol. Cancer *18*, 46.

21. Hu, X., Peng, W.-X., Zhou, H., Jiang, J., Zhou, X., Huang, D., Mo, Y.-Y., and Yang, L. (2019). IGF2BP2 regulates DANCR by serving as an N6-methyladenosine reader. Cell Death Differ. Published online December 5, 2019. https://doi.org/10.1038/s41418-019-0461-z.

22. Zhao, W., Cui, Y., Liu, L., Qi, X., Liu, J., Ma, S., et al. (2020). Splicing factor derived circular RNA circUHRF1 accelerates oral squamous cell carcinoma tumorigenesis via feedback loop. Cell Death Differ. *27*, 919–933.

23. Vu, L.P., Pickering, B.F., Cheng, Y., Zaccara, S., Nguyen, D., Minuesa, G., Chou, T., Chow, A., Saletore, Y., MacKay, M., et al. (2017). The N^6-methyladenosine (m^6A)-forming enzyme METTL3 controls myeloid differentiation of normal hematopoietic and leukemia cells. Nat. Med. *23*, 1369–1376.

24. Chen, X.Y., Zhang, J., and Zhu, J.S. (2019). The role of m^6A RNA methylation in human cancer. Mol. Cancer *18*, 103.

25. Wu, J., Qi, X., Liu, L., Hu, X., Liu, J., Yang, J., Yang, J., Lu, L., Zhang, Z., Ma, S., et al. (2019). Emerging Epigenetic Regulation of Circular RNAs in Human Cancer. Mol. Ther. Nucleic Acids *16*, 589–596.

26. Wu, J., Zhao, W., Wang, Z., Xiang, X., Zhang, S., and Liu, L. (2019). Long non-coding RNA SNHG20 promotes the tumorigenesis of oral squamous cell carcinoma via targeting miR-197/LIN28 axis. J. Cell. Mol. Med. *23*, 680–688.

27. Li, Y., Wu, K., Quan, W., Yu, L., Chen, S., Cheng, C., Wu, Q., Zhao, S., Zhang, Y., and Zhou, L. (2019). The dynamics of FTO binding and demethylation from the m(6)A motifs. RNA Biol. *16*, 1179–1189.

28. Li, T., Hu, P.S., Zuo, Z., Lin, J.F., Li, X., Wu, Q.N., Chen, Z.H., Zeng, Z.L., Wang, F., Zheng, J., et al. (2019). METTL3 facilitates tumor progression via an m^6A-IGF2BP2-dependent mechanism in colorectal carcinoma. Mol. Cancer *18*, 112.

29. He, H., Wu, W., Sun, Z., and Chai, L. (2019). MiR-4429 prevented gastric cancer progression through targeting METTL3 to inhibit m(6)A-caused stabilization of SEC62. Biochem. Biophys. Res. Commun. *517*, 581–587.

30. Nicklas, S., Hillje, A.L., Okawa, S., Rudolph, I.M., Collmann, F.M., van Wuellen, T., Del Sol, A., and Schwamborn, J.C. (2019). A complex of the ubiquitin ligase TRIM32 and the deubiquitinase USP7 balances the level of c-Myc ubiquitination and thereby determines neural stem cell fate specification. Cell Death Differ. *26*, 728–740.

31. Jen, J., Liu, C.Y., Chen, Y.T., Wu, L.T., Shieh, Y.C., Lai, W.W., and Wang, Y.C. (2019). Oncogenic zinc finger protein ZNF322A promotes stem cell-like properties in lung cancer through transcriptional suppression of c-Myc expression. Cell Death Differ. *26*, 1283–1298.

32. Lin, X., Chai, G., Wu, Y., Li, J., Chen, F., Liu, J., Luo, G., Tauler, J., Du, J., Lin, S., et al. (2019). RNA m^6A methylation regulates the epithelial mesenchymal transition of cancer cells and translation of Snail. Nat. Commun. *10*, 2065.

33. Chen, M., Wei, L., Law, C.T., Tsang, F.H., Shen, J., Cheng, C.L., Tsang, L.H., Ho, D.W., Chiu, D.K., Lee, J.M., et al. (2018). RNA N6-methyladenosine methyltransferase-like 3 promotes liver cancer progression through YTHDF2-dependent posttranscriptional silencing of SOCS2. Hepatology *67*, 2254–2270.

34. Li, Z., Weng, H., Su, R., Weng, X., Zuo, Z., Li, C., Huang, H., Nachtergaele, S., Dong, L., Hu, C., et al. (2017). FTO Plays an Oncogenic Role in Acute Myeloid Leukemia as a N^6-Methyladenosine RNA Demethylase. Cancer Cell *31*, 127–141.